Imaging the Elastic Properties of Coiled Carbon Nanotubes with Atomic Force Microscopy

A. Volodin, M. Ahlskog, E. Seynaeve, and C. Van Haesendonck
Laboratorium voor Vaste-Stoffysica en Magnetisme, Katholieke Universiteit Leuven, Celestijnenlaan 200 D, B-3001 Leuven, Belgium

A. Fonseca and J. B. Nagy
Laboratoire de Résonance Magnétique Nucléaire, Facultés Universitaires Notre-Dame de la Paix, Rue de Bruxelles 61, B-5000 Namur, Belgium
(Received 7 June 1999; revised manuscript received 17 December 1999)

Coiled carbon nanotubes were produced catalytically by thermal decomposition of hydrocarbon gas. After deposition on a silicon substrate, the three-dimensional structure of the helix-shaped multiwalled nanotubes can be visualized with atomic force microscopy. Helical structures of both chiralities are present in the nanotube deposits. For larger coil diameters (>170 nm), force modulation microscopy allows one to probe the local elasticity along the length of the coil. Our results agree with the classical theory of elasticity. Similar to the case of straight nanotubes, the Young modulus of coiled multiwalled nanotubes remains comparable to the very high Young modulus of hexagonal graphene sheets.

PACS numbers: 61.48.+c, 61.16.Ch, 62.20.Dc

While carbon nanotubes are known to easily bend due to external factors such as substrate obstacles, intrinsically curved carbon nanotubes have been observed as well. Intrinsically coiled nanotubes have been observed in deposits of catalytically grown material [1]. The helices exhibit a regular structure with a coil diameter and pitch ranging from 10 nm to 1 μm. Carbon nanotube rings with typical diameter of 500 nm appear in single walled nanotube (SWNT) and in multiwalled nanotube (MWNT) deposits [2–4]. Because of the large nanotube elasticity, the van der Waals interaction with the substrate is able to stabilize the ring structures [4].

The intrinsic curvature of catalytically grown nanotubes is likely to occur without a very large elastic strain being involved. At this point, it is not clear whether a coiled growth mechanism involves the presence of specific atomic scale defects. High resolution transmission electron microscopy of coiled MWNTs [1] suggests that these tubes are polygonized, and consist of short straight segments. The coiling can result from the introduction of pentagon-heptagon pairs at regular distances in the hexagonal network forming the wall of a straight carbon nanotube [5]. The question remains why such defects appear periodically to form the helical structure [6].

Here, we present the first observation with an atomic force microscope (AFM) of parts of longer coiled MWNTs which have been deposited on an oxidized silicon substrate. Sometimes, the regular pitch of the helix shape is preserved after deposition, despite the forces that are involved in the breaking of the helix and the van der Waals interaction with the substrate. Reliable imaging is possible only in the noncontact mode or in the tapping mode. The coils are weakly bonded to the substrate and start to move when the interaction with the silicon cantilever is increased above 1 nN. We have used force modulation microscopy (FMM) [7] in the tapping mode of operation to study variations in the elastic response of the coils along their length. Our results nicely agree with the classical theory of elasticity. From our FMM measurements we infer a Young modulus around 0.7 TPa for the coiled MWNTs. This result is consistent with the reported high values of Young's modulus for straight carbon nanotubes which has been measured via resonant motion [8,9] of free standing tubes as well as via AFM induced deformations of nanotubes deposited on a flat surface [10] or on substrates containing micropores [11].

The nanotube material containing the helical MWNTs is produced by catalytic decomposition of acetylene, carried out at 700 °C in a flow reactor at atmospheric pressure [12]. The purified carbon nanotube material is sonicated at low power in isopropanol and is deposited onto a piece of an oxidized silicon wafer with gold markers fabricated by combining electron beam lithography and lift-off techniques. The nanotube deposits are first imaged with a scanning electron microscope (SEM: Philips, XL-30 FEG), allowing one to record the position of the coiled structures. Next, the AFM imaging and the FMM measurements are performed in air with a commercial system (Park Scientific Instruments, M5) using silicon cantilevers with a tip apex radius of curvature of about 10 nm. The elastic response of the coiled nanotubes can be probed locally with the FMM technique [7] which is illustrated in Fig. 1(a). The Si cantilever is gently tapping the sample surface at the cantilever resonance frequency $f_{\mathrm{res}} \simeq 98$ kHz with an amplitude ranging between 0.2 and 5 nm. Additionally, the vertical position of the sample is periodically modulated at a much smaller frequency f_{mod} in the range 8–11 kHz with a modulation amplitude between 1 and 2 nm. Harmonic detection at the frequency f_{mod} of the periodically varying interaction between tip and coiled nanotube enables one to locally probe its elasticity.

 0031-9007/00/84(15)/3342(4)$15.00

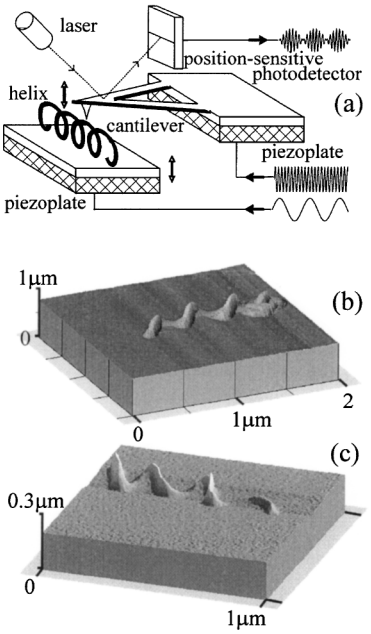

FIG. 1. (a) Schematic view of the force modulation microscopy (FMM) measurements. In (b) and (c) we show AFM images of the helix-shaped nanotubes CNT-1 and CNT-2 (see Table I), revealing both types of chirality.

Although we frequently observe with the SEM coiled nanotubes which are attached to the oxidized Si substrate, many of them cannot be reliably imaged with the AFM because they are surrounded by other carbon material or because of their poor adhesion to the substrate. On the other hand, many of the helix-shaped tubes have a pitch and diameter which is too small to allow the penetration of the AFM tip in between the windings. We will concentrate on the AFM and FMM results for three coiled MWNTs having a coil diameter $2R > 170$ nm. Table I gives an overview of these MWNTs with tube diameter $2r$.

Figures 1(b) and 1(c) show three-dimensional noncontact AFM images of the coiled nanotubes CNT-1 and CNT-2 listed in Table I. The AFM images offer the possibility to unambiguously determine the chirality of the helix-shaped nanotubes as either right-handed or left-handed. Figures 1(b) and 1(c) confirm that both chiralities indeed occur. In Fig. 2(a) we show the SEM image of sample CNT-1. In Fig. 2(b) we show a topographical AFM image of this sample which has been obtained in the tapping mode of operation and has been recorded simultaneously with the FMM image shown in Fig. 2(c).

TABLE I. Relevant parameters of the coiled nanotubes which have been studied in detail.

Sample	CNT-1			CNT-2			CNT-3		
Winding	1	2	3	1	2	3	1	2	3
$2r$ (nm)	27	27	27	22	22	22	33	33	33
$2R$ (nm)	200	200	170	190	170	190	580	370	310
E (TPa)	0.6	0.8	0.6	0.7	0.4	0.9	0.4	0.7	0.6

In the FMM image the lightest areas correspond to the stiffest parts of the nanotube windings. Each of the windings makes contact to the substrate only along a small segment (arclength $<30°$) which appears as stiff as the surrounding substrate. Because of the helix-shaped structure, the interaction strength with the oxidized silicon substrate will obviously be smaller than for straight nanotubes. While both the SEM [Fig. 2(a)] and the AFM [Fig. 2(b)] images are consistent with a diameter of the helix close to 200 nm, the AFM image of the tube is considerably smeared out because of the finite size of the AFM tip. On the other hand, the excellent depth resolution of the AFM images is absent for the SEM images which cannot provide any conclusive information concerning the chirality of the coiled nanotubes.

In order to obtain quantitative information from our FMM data, we rely on the simple model illustrated in Fig. 3(a), where a winding of the helix structure is approximated as a thin circular beam which is clamped to a substrate along a short segment. In Fig. 3(c) we plot the variation of the FMM signal acquired for sample CNT-1 along the upper part [cross section x_1 in Fig. 2(c)] and the lower part [cross section x_2 in Fig. 2(c)] of a winding of the helix. For comparison we show in Fig. 3(b) the corresponding AFM topography which does not reflect the sample elasticity. The FMM signal, which is proportional to the local elastic spring constant k, is normalized with respect to the response measured at the top of the winding ($x_1 = 0$). The data plotted in Fig. 3(c) illustrate the large difference between the elastic compliance of the upper parts of the helical nanotube and of the silicon substrate. On the other hand, the elastic response of the lowest parts, where the nanotube is attached to the substrate, is comparable to the response of the substrate. This can be understood in terms of the classical Hertz model for the interaction between the tip and the deposited nanotube [13], taking into account the high Young modulus of the nanotube [10].

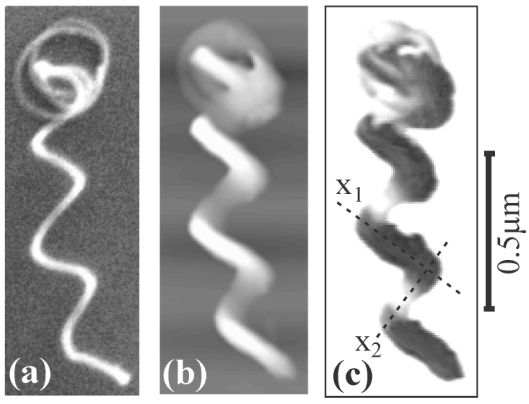

FIG. 2 (a) Electron micrograph of CNT-1. In (b) we show the topographic AFM image recorded simultaneously with the FMM image shown in (c).

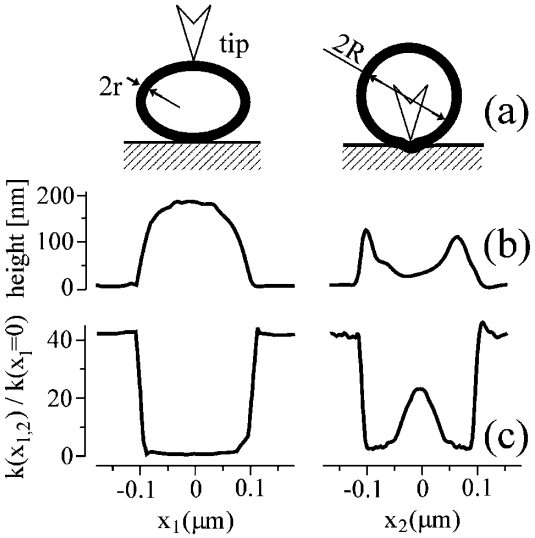

FIG. 3 (a) The circular beam approximation which is used to model the elastic response of a single winding of a coiled nanotube. (b) AFM topography of the upper part and the lower part of a winding of CNT-1 [cross sections x_1 and x_2 in Fig. 2(c), respectively]. (c) Corresponding spatial dependence of the normalized stiffness.

Referring to the schematic picture shown in Fig. 3(a), the variation of the spring constant along the upper part of the circular beam can be expressed in terms of the local coordinate x_1 [14]:

$$k(x_1) = \frac{2\pi EI}{(4-\pi)R^3}\left[1-\left(\frac{x_1}{\pi R}\right)^2\right]^{-2}, \qquad (1)$$

where E is the Young modulus and $I = \pi r^4/4$ is the moment of inertia. Equation (1) results from a series expansion which reproduces the exact result within 10% for $|x_1| < 0.7R$. Figure 4(a) shows the measured variations of the stiffness near the top of the windings of sample CNT-1 (full curves) and near the top of winding 1 (see Table I) of CNT-3 (dotted curve). The FMM data have been averaged over 256 (CNT-1) and 16 (CNT-3) different scans in order to improve the signal-to-noise ratio. The FMM data have also been scaled according to the size-dependent prefactor in Eq. (1). The scaled FMM data agree with the x_1 dependence predicted by Eq. (1) (dashed curves).

Figure 4(b) shows the detailed variation of the normalized elastic spring constant near the bottom of a winding of sample CNT-1 [cross section x_2 in Fig. 2(c)]. The highest rigidity is detected near $x_2 = 0$, i.e., for the attached segment of the nanotube. The observed decrease of $k(x_2)$ with increasing x_2 fits a $|x_2 - x_c|^{-3}$ dependence with $x_c = 8$ nm. Such a dependence is expected for small distances $|x_2 - x_c|$ [14].

A quantitative estimate of the Young modulus of the helical MWNTs can in principle be obtained from a comparison of the elastic response of the nanotubes and of the silicon substrate, respectively. Such a direct comparison

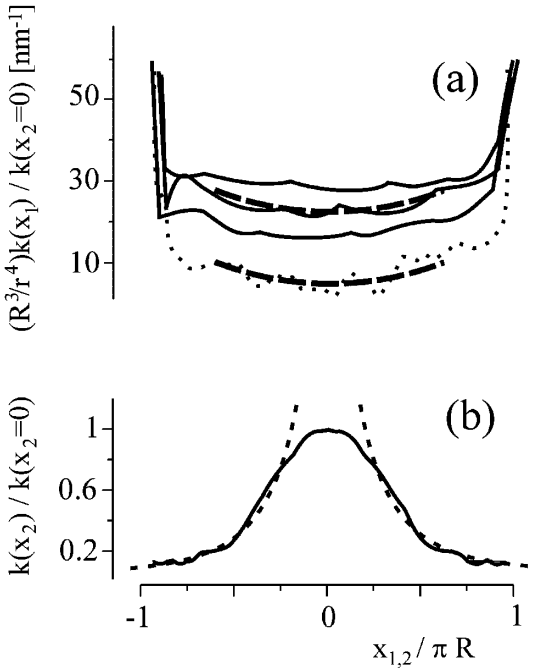

FIG. 4. (a) Variation of the normalized stiffness along the upper part of the three windings of CNT-1 (solid lines) and along the upper part of winding 1 (see Table I) of CNT-3 (dotted line). The dashed curves represent fits corresponding to Eq. (1). (b) Spatial dependence of the normalized stiffness near the bottom of a winding of CNT-1 [cross section x_2 in Fig. 2(c)]. The dashed line represents a fit illustrating the $|x_2 - x_c|^{-3}$ dependence of the stiffness.

turns out to be less reliable because of an uncontrolled difference in the tapping parameters for the nanotubes and the substrate. In order to overcome this problem, we compare the compliance of the free standing parts of the windings to the compliance of the attached segments of the MWNT. We assume that the Young modulus of the coiled nanotubes is considerably larger than the Young modulus of the substrate and of the tip. According to the Hertz model, the effective spring constant of the tip-sample contact near $x_2 = 0$ is then given by [13]

$$k_e(x_2 = 0) = \frac{2E_{\mathrm{Si}}}{1-\nu_{\mathrm{Si}}^2}\sqrt{r_e z}\,. \qquad (2)$$

$\nu_{\mathrm{Si}} = 0.217$ and $E_{\mathrm{Si}} = 166$ Gpa are the Poisson ratio and the Young modulus of silicon, respectively. The effective radius of the contact, r_e, is of the order of 10 nm, i.e., comparable to both the nanotube radius r and the tip apex radius of curvature. Since we are neglecting radial nanotube deformations near $x_2 = 0$, the vertical deformation, z, corresponds to the sum of the deformations of the tip and substrate, respectively.

The validity of the Hertz model for describing the elastic response of the attached parts of the nanotubes is illustrated in Fig. 5. In Fig. 5 we plot on a double logarithmic scale the dependence of the normalized spring constant on the normalized deformation for different settings of the oscillation amplitude (following the procedure

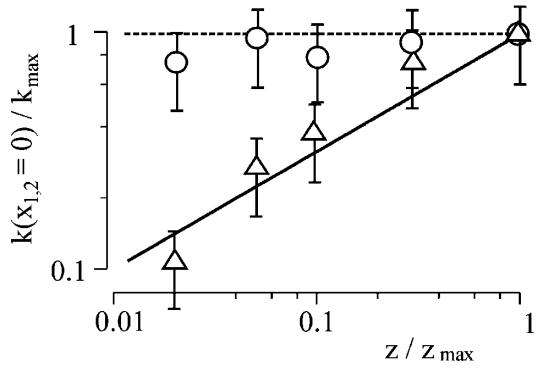

FIG. 5. Normalized elastic spring constant versus normalized deformation for the top (circles) and the bottom (triangles) of winding 2 (see Table I) of CNT-1. As illustrated by the full line, the observed variation for the bottom of the winding agrees with the Hertz model [see Eq. (2)].

outlined in [13]). The data have been obtained for sample CNT-1 at $x_1 = 0$ and $x_2 = 0$. For the attached part of the nanotube the dependence on the deformation agrees with the $\sqrt{z}$ dependence predicted by Eq. (2) (full line in Fig. 5). On the other hand, for the upper part of the nanotube winding the stiffness is independent of the deformation (dashed curve in Fig. 5).

The Hertz approximation allows us to translate our FMM data into absolute values for the local elastic spring constant. The Young modulus E of the coiled carbon nanotubes can then be obtained from Eq. (1). The calculated E values are listed in Table I. Our results reveal that the Young modulus is very high for helix-shaped MWNTs with a helix diameter of 170 nm or larger. This agrees with previous measurements on straight MWNTs prepared by the arc-discharge method [10] and by pyrolysis of acetylene [15]. We conclude that the helical shape of our MWNTs does not have a large influence on the elastic properties which are still governed by the very high Young modulus of hexagonal graphene sheets [5].

In conclusion, atomic force microscopy and force modulation microscopy in the tapping mode can be used to characterize the three-dimensional structure and the elastic properties of coiled multiwalled carbon nanotubes deposited on oxidized silicon substrates. The AFM images unambiguously confirm the existence of two different chiralities for the helix-shaped nanotubes. Our force modulation measurements allow one to probe spatial variations of the elastic response of the coiled nanotubes. The helix-shaped nanotubes make contact to the substrate only along a small segment of each of the windings. We obtain a value for the Young modulus which is consistent with the very high Young modulus of hexagonal graphene sheets. Future experiments will focus on the mechanical resonances of the helix-shaped carbon nanotubes which should behave as nanosprings.

The work at the K. U. Leuven has been supported by the Fund for Scientific Research-Flanders (FWO) and by the Flemish Concerted Action (GOA) program. The collaboration between the FUNDP Namur and the K. U. Leuven has been funded by the Belgian Inter-University Attraction Poles (IUAP) program on Reduced Dimensionality Systems (PAI-IUAP No. 4/10).

[1] X. B. Zhang *et al.,* Europhys. Lett. **27,** 141 (1994).
[2] J. Liu *et al.,* Nature (London) **385,** 780 (1997).
[3] M. Ahlskog *et al.,* Chem. Phys. Lett. **300,** 202 (1999).
[4] R. Martel, H. R. Shea, and Ph. Avouris, Nature (London) **398,** 299 (1999).
[5] D. H. Robertson, D. W. Brenner, and J. W. Mintmire, Phys. Rev. B **45,** 12 592 (1992).
[6] B. I. Dunlap, Phys. Rev. B **50,** 8134 (1994).
[7] P. Maivald *et al.,* Nanotechnology **2,** 103 (1991).
[8] M. M. Treacy, T. W. Ebbesen, and J. M. Gibson, Nature (London) **381,** 678 (1996).
[9] P. Poncharal *et al.,* Science **283,** 1513 (1999).
[10] E. Wong, P. Sheehan, and C. Lieber, Science **277,** 1971 (1997).
[11] J.-P. Salvetat *et al.,* Phys. Rev. Lett. **82,** 944 (1999).
[12] K. Hernadi *et al.,* Zeolites **17,** 416 (1996).
[13] R. G. Winkler *et al.,* Phys. Rev. B **54,** 8908 (1996).
[14] B. M. Fraeijs de Veubeke, *A Course in Elasticity* (Springer-Verlag, New York, 1979).
[15] Z. W. Pan *et al.,* Appl. Phys. Lett. B **74,** 3152 (1999).